Theory of the nondegenerate two-photon micromaser

P. A. Maia Neto and L. Davidovich
Departamento de Física, Pontifícia Universidade Católica do Rio de Janeiro, Caixa Postal 38071, 22452 Rio de Janiero RJ, Brazil

J. M. Raimond
Laboratoire de Spectroscopie Hertzienne, Ecole Normale Supérieure, 24, rue Lhomond, 75231 Paris CEDEX 5, France

(Received 2 October 1990)

We present the theory of a microscopic maser operating on a nondegenerate two-photon transition between two states of same parity. We start from a three-level Hamiltonian, and discuss both the one-photon resonant cascade and the two-photon regime, when the intermediate state is far off resonance. In the semiclassical limit, we derive rate equations for the field intensities and get the corresponding steady-state values. The vacuum is stable in the two-photon regime but becomes unstable for zero detuning (a clear signature of a one-photon process). Solutions displaying true two-photon operation (intermediate state unpopulated) even with zero detuning are displayed. Using the full quantum density-matrix approach, we derive a master equation for the field and discuss both operating regimes, showing that the spontaneous emission may turn the vacuum unstable in the two-photon case. In the off-resonance two-photon regime, there is a strong correlation between the fluctuations of the intensities of the two modes. We find a squeezing factor of 50% for the fluctuations in the difference of intensities.

I. INTRODUCTION

Micromasers are quantum oscillators operating on a Rydberg atomic transition (high principal quantum numbers), where the initially excited atoms interact with the electromagnetic field while crossing a high-Q superconducting cavity. Very low thresholds may be attained, down to at most one atom in the cavity at a time.[1–5] These devices provide experimental tests of some very fundamental models of quantum optics, and exhibit a great variety of interesting quantum effects, like collapses and revivals,[6] generation of sub-Poissonian states,[1–5] trapping states,[7,8] spontaneous self-starting,[5] and singular starting times.[9]

Furthermore, they have allowed the operation of the first two-photon oscillator,[2] involving a degenerate two-photon transition between two atomic levels of the same parity. This device presents additional interesting features, with respect to the one-photon micromaser, which are connected to the starting up of the system.[10] Classically, the zero-field state is always stable, even if one is above the oscillation threshold (an injected field is thus required, in order for the system to build up the oscillation.) Quantum fluctuations may, however, render this state metastable or even unstable, thus inducing the system to start oscillating, without need of any triggering field, in a time which, for micromasers, may be very small.[2,5]

Up to now, only the degenerate case has been analyzed, both theoretically[4,5] and experimentally.[2] For this reason, one has missed one of the important features of the two-photon process, namely, the correlation between the two photons emitted simultaneously into two different modes. Such correlations have been studied in optical parametric oscillators, where an important noise reduction in the difference of intensities of the two modes has been demonstrated.[11,12]

In this paper, we extend the previous analysis[4,5] to a more general situation, where the two photons are emitted into different modes of the cavity (nondegenerate two-photon transition). We base our treatment on a full three-level model, instead of a two-level effective Hamiltonian. In this way, conditions under which the effective-Hamiltonian approach is valid can be precisely stated. We show that, contrary to the laser case,[13,14] the three-level model does not introduce any substantial correction, in the high-detuning region. On the other hand, it allows one to go continuously from the two-photon operating regime (corresponding to the high-detuning limit—no population in the intermediate state) to the one-photon resonant cascade process, in which the intermediate state gets populated.

We consider thus a three-level atom (Fig. 1), with the upper and lower levels having the same parity. We assume that the atomic lifetimes are much larger than the time of flight of the atoms through the cavity, t_{int}. Therefore, the atoms do not decay while crossing the cavity. We also assume that the two cavity modes (frequencies ω_1 and ω_2) are coupled, respectively, to the upper and lower transitions, so that we neglect the process in which the two photons are emitted in reverse order (the photon with frequency ω_2 corresponding to the upper transition). In Sec. II, we show that in order for this to be true, one must have

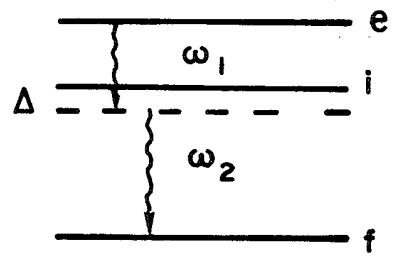

FIG. 1. Energy levels relevant to the nondegenerate two-photon micromaser.

$$|\omega_1-\omega_2| \gg \Delta,\Gamma \ , \tag{1.1}$$

where Γ is the linewidth of the one-photon transition to the intermediate state, and

$$\Delta=\omega_1-(E_e-E_i)/\hbar \tag{1.2}$$

is the detuning between the intermediate state $|i\rangle$ and the energy reached after the emission of the first photon (see Fig. 1). Equation (1.1) implies that the degenerate case cannot be obtained as a limit of the present model. On the other hand, we consider the general situation where Δ can assume any value, including the case of zero detuning (one-photon cascade maser regime). We pay special attention, however, to the large detuning regime, in which two-photon transitions without population transfer to the state $|i\rangle$ are expected (the intermediate state acts then as a virtual state). In this case, we show rigorously that an effective two-level Hamiltonian may be adopted.

In this two-photon regime, each atomic transition creates simultaneously one photon in each mode, so that one expects a strong quantum correlation between the modes. We show indeed that the variance of the difference of intensities of the two modes is well below the classical lower bound (up to 50%), thus providing a clear signature of that correlation.

This paper is organized in the following way. In Sec. II we write down the Hamiltonian for the atom-field system and solve the resulting equations for the probability amplitudes of the atom-field states. The corresponding transition probabilities are then used to get the gain terms in the field master equation. Adding the cavity losses, we obtain the dynamical equations both in the semiclassical approximation (Sec. III), where we neglect the field fluctuations and the spontaneous emission, and in the full quantum approach (Sec. IV), from which we get some exact and numerical results concerning the field statistical distribution. In the semiclassical approximation, we find a class of solutions for which the micromaser oscillates in the true two-photon regime, the intermediate state remaining unpopulated, even with zero detuning. In the quantum theory, we make a detailed analysis of the stability of the zero-field state and of the time-dependent behavior of the system, and we display the quantum correlations between the two modes. A general discussion of our results, as well as the concluding remarks, are presented in Sec. V.

II. THE ATOM-FIELD HAMILTONIAN: TIME EVOLUTION OF THE PROBABILITY AMPLITUDES

We calculate in this section the probability amplitudes which describe the transitions between the three atomic levels for the system depicted in Fig. 1. The corresponding Hamiltonian has the form

$$H=H_{\rm at}+H_F+H_{\rm int} \ , \tag{2.1}$$

where

$$H_{\rm at}=E_e|e\rangle\langle e|+E_i|i\rangle\langle i|+E_f|f\rangle\langle f| \ , \tag{2.2}$$

$$H_F=\hbar\omega_1 a_1^\dagger a_1+\hbar\omega_2 a_2^\dagger a_2 \ , \tag{2.3}$$

and $a_i, a_i^\dagger$ are the annihilation and creation operators for mode i ($i=1,2$).

If we neglect the couplings of the upper and lower atomic transitions with modes 2 (frequency ω_2) and 1 (frequency ω_1), respectively, we get for $H_{\rm int}$ in the rotating-wave approximation

$$H_{\rm int}=\hbar\Omega_{ei}a_1|e\rangle\langle i|+\hbar\Omega_{if}a_2|i\rangle\langle f| +\hbar\Omega_{ei}a_1^\dagger|i\rangle\langle e|+\hbar\Omega_{if}a_2^\dagger|f\rangle\langle i| \ , \tag{2.4}$$

where

$$\hbar\Omega_{ei}=-\langle e|\hat{D}|i\rangle\sqrt{\hbar\omega_1/2\epsilon_0 V} \ , \tag{2.5}$$

$$\hbar\Omega_{if}=-\langle i|\hat{D}|f\rangle\sqrt{\hbar\omega_2/2\epsilon_0 V} \ , \tag{2.6}$$

$\hat{D}$ is the dipole operator and V is the effective volume of modes 1 and 2 (assumed to be the same for both modes).

The neglected couplings are proportional to $a_2|e\rangle\langle i|$ and $a_1|i\rangle\langle f|$, which, in the interaction picture, become $\exp[i(\omega_1-\omega_2-\Delta)t]a_2|e\rangle\langle i|$ and $\exp[i(\omega_2-\omega_1+\Delta)t]a_1|i\rangle\langle f|$. They are therefore nonresonant and negligible compared to $\exp(-i\Delta t)a_1|e\rangle\langle i|$, $\exp(i\Delta t)a_2|i\rangle\langle f|$, if condition (1.1) holds. Neglecting these terms corresponds to a generalized rotating-wave approximation, where besides the usual condition involving the transition linewidth Γ, one has a new one concerning the detuning Δ. This hypothesis simplifies the solution of the problem, since then triplets $|e,N_1,N_2\rangle$, $|i,N_1+1,N_2\rangle$, $|f,N_1+1,N_2+1\rangle$ corresponding to different values of N_1 or N_2 become decoupled. Consequently, the Schrödinger equation needs to be solved only within this three-dimensional space.

A general state in this space can be written as

$$|\psi(t)\rangle=a(N_1,N_2,t)|e,N_1,N_2\rangle +b(N_1+1,N_2,t)|i,N_1+1,N_2\rangle +c(N_1+1,N_2+1,t)|f,N_1+1,N_2+1\rangle \ . \tag{2.7}$$

In the interaction picture, the Schrödinger equation is

$$i\hbar\frac{\partial|\psi\rangle}{\partial t}=\tilde{H}_{\rm int}|\psi\rangle \ , \tag{2.8}$$

where

$$\tilde{H}_{\rm int}=\hbar\Omega_{ei}e^{-i\Delta t}a_1|e\rangle\langle i| +\hbar\Omega_{if}e^{i\Delta t}a_2|i\rangle\langle f|+\text{H.c.} \tag{2.9}$$

From (2.7), (2.8), and (2.9), we get then the following equations for the probability amplitudes:

$$i\partial a(N_1,N_2,t)/\partial t=\Omega_{ei}b(N_1+1,N_2,t)\sqrt{N_1+1}e^{-i\Delta t}\ , \tag{2.10a}$$

$$i\partial b(N_1+1,N_2,t)/\partial t=\Omega_{if}c(N_1+1,N_2+1,t)\sqrt{N_2+1}e^{i\Delta t}+\Omega_{ei}a(N_1,N_2,t)\sqrt{N_1+1}e^{i\Delta t}\ , \tag{2.10b}$$

$$i\partial c(N_1+1,N_2+1,t)/\partial t=\Omega_{if}b(N_1+1,N_2,t)\sqrt{N_2+1}e^{-i\Delta t}\ . \tag{2.10c}$$

These equations are solved by Laplace transform techniques, following the method of Ref. 14. The detailed solution is presented in Appendix A. The final result for $b(N_1+1,N_2,t)$ and $c(N_1+1,N_2+1,t)$, with the initial conditions $a(0)=1$, $b(0)=c(0)=0$, is

$$c(N_1+1,N_2+1,t)=\frac{\Omega_{ei}\sqrt{N_1+1}\Omega_{if}\sqrt{N_2+1}\{[\cos\Omega t+(i\Delta/2\Omega)\sin\Omega t]e^{-i\Delta t/2}-1\}}{\Omega^2-(\Delta/2)^2}\ , \tag{2.11}$$

$$b(N_1+1,N_2,t)=-i(\Omega_{ei}/\Omega)\sqrt{N_1+1}e^{i\Delta t/2}\sin\Omega t\ , \tag{2.12}$$

where

$$\Omega=[\Omega_{ei}^2(N_1+1)+\Omega_{if}^2(N_2+1)+\Delta^2/4]^{1/2}\ . \tag{2.13}$$

The corresponding transition probabilities are

$$|c(N_1+1,N_2+1,t)|^2=\frac{\Omega_{ei}^2(N_1+1)\Omega_{if}^2(N_2+1)}{[\Omega_{ei}^2(N_1+1)+\Omega_{if}^2(N_2+1)]^2}\{\cos^2\Omega t+(\Delta/2\Omega)^2\sin^2\Omega t+1$$
$$-2[\cos\Omega t\cos(\Delta t/2)+(\Delta/2\Omega)\sin\Omega t\sin(\Delta t/2)]\}\ , \tag{2.14}$$

$$|b(N_1+1,N_2,t)|^2=\frac{\Omega_{ei}^2(N_1+1)}{\Omega^2}\sin^2\Omega t\ . \tag{2.15}$$

The quantity $|b|^2(|c|^2)$ is the probability for finding the atom in the state $|i\rangle$ ($|f\rangle$), assuming it was in the excited state $|e\rangle$ in $t=0$, while the field was in the Fock state $|N_1\rangle\otimes|N_2\rangle$. These probabilities behave very differently in two opposite limits.

(a) Zero detuning: $\Delta=0$. In this case, $|b|^2$ is proportional to $\sin^2\Omega t$, while $|c|^2$ becomes proportional to $\sin^4(\Omega t/2)$, meaning that for $t\ll\Omega^{-1}$, $|b|^2\gg|c|^2$, which is not surprising; before it reaches $|f\rangle$, the atom has to evolve through the intermediate state $|i\rangle$ in a time of the order of the Rabi period $2\pi\Omega^{-1}$.

(b) Large detuning:

$$\Delta\gg\frac{\Omega_{ei}^2(N_1+1)+\Omega_{if}^2(N_2+1)}{\Delta}\ . \tag{2.16}$$

In this case,

$$|b(N_1+1,N_2+1,t)|^2=O(\Omega_{ei}^2(N_1+1)/\Delta^2)\to 0\ ,$$

while

$$|c(N_1+1,N_2+1,t)|^2\to\frac{2\Omega_{ei}^2(N_1+1)\Omega_{if}^2(N_2+1)}{[\Omega_{ei}^2(N_1+1)+\Omega_{if}^2(N_2+1)]^2}(1-\cos\Omega_{2\gamma}t_{\rm int})\ , \tag{2.17}$$

where

$$\Omega_{2\gamma}=\frac{\Omega_{ei}^2(N_1+1)+\Omega_{if}^2(N_2+1)}{\Delta} \tag{2.18}$$

is the two-photon Rabi frequency, with the well-known typical properties of a two-photon process:[4,5] proportional to the intensities, inversely proportional to the detuning Δ. It is quite similar to the two-photon degenerate Rabi frequency and may be more easily derived by using the techniques of Ref. 4. In fact, in this limit, the intermediate state participates only virtually, and it can be taken into account by perturbation theory (see Fig. 2), since then the coupling within the degenerate doublet $\{|e,N_1,N_2\rangle,|f,N_1+1,N_2+1\rangle\}$ is much more important. In the dressed-atom approach, the dressed states and energies are the eigenvectors and eigenvalues of the 2×2 matrix

$$\begin{bmatrix} \dfrac{-\Omega_{ei}^2(N_1+1)}{\Delta} & \dfrac{-\Omega_{ei}\sqrt{N_1+1}\Omega_{if}\sqrt{N_2+1}}{\Delta} \\ \dfrac{-\Omega_{ei}\sqrt{N_1+1}\Omega_{if}\sqrt{N_2+1}}{\Delta} & \dfrac{-\Omega_{if}^2(N_2+1)}{\Delta} \end{bmatrix}\ .$$

The diagonal elements of the matrix are the Stark shifts of the states $|e\rangle$ and $|f\rangle$; we see that this effect may be much more important here than in the degenerate case. Even if $\Omega_{ei}=\Omega_{if}$, it may produce a large effective detuning if $N_1\neq N_2$, thus lowering the transition probability when the intensities are different. Indeed, for $\Omega_{ei}=\Omega_{if}$, we may write the transition probability in the following form:

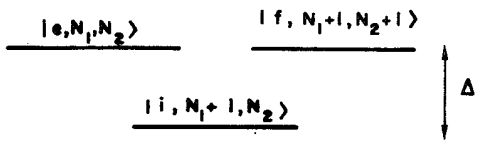

FIG. 2. Energy diagram of the noninteracting atom-field system.

$$|c|^2=[1-(N_1-N_2)^2/(N_1+N_2+2)^2]\times\sin^2[\Omega_{ei}^2(N_1+N_2+2)t/2\Delta]\ , \tag{2.19}$$

which displays the out-of-resonance reduction of the Rabi nutation amplitude.

The transition probabilities calculated in this section will now be used to develop both the semiclassical and the quantum theory of the nondegenerate two-photon micromaser.

III. SEMICLASSICAL THEORY

We develop in this section the semiclassical theory of the nondegenerate two-photon micromaser. In Fig. 3, we display the basic parameters of this device: t_{at} is the average time interval between consecutive excited atoms entering the cavity, t_{int} is, as mentioned before, the time of flight of the atoms through the cavity, and t_{cav_1}, t_{cav_2} are the cavity damping times for modes 1 and 2. We assume that $t_{at}\geq t_{int}$, so that in the average only one atom at most interacts with the field at any time (micromaser condition). The average gain G in each mode is given by the product of the average atomic rate (t_{at}^{-1}) by the average transition probability:

$$G(\text{mode 1})=t_{at}^{-1}\langle|b|^2+|c|^2\rangle\ ,$$

$$G(\text{mode 2})=t_{at}^{-1}\langle|c|^2\rangle\ ,$$

where the average $\langle\ \rangle$ is taken over the field density-matrix operator.

Each photon in the lower mode is emitted together with an upper-mode photon, but the converse is not generally true. Therefore, as we see above, the gain for the upper mode is larger than the gain for the lower one, except in the situations where the atoms never leave the cavity in the intermediate state. The most important exception is associated with the large-detuning limit, where the intermediate state is out of resonance [Eq. (2.16)]. However, even in the resonant case there are some few regimes of oscillation where the gains are equal. We illustrate this effect when we discuss the zero-detuning case ($\Delta=0$), which follows the large-detuning limit discussion. We analyze therefore two opposite limits.

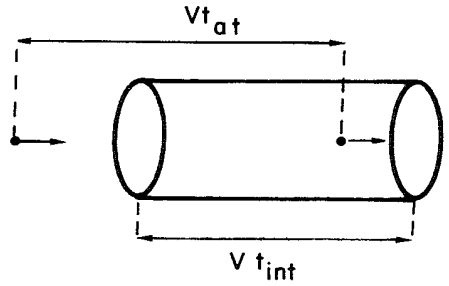

FIG. 3. Sketch of the micromaser setup.

(a) Large detuning:

$$\Delta\gg[\Omega_{ei}^2(N_1+1)+\Omega_{if}^2(N_2+1)]/\Delta\ .$$

The two-photon probability is given by (2.17). Then

$$G(\text{mode 1})=G(\text{mode 2})=\frac{1}{t_{at}}\left[\frac{2\Omega_{ei}^2(N_1+1)\Omega_{if}^2(N_2+1)}{[\Omega_{ei}^2(N_1+1)+\Omega_{if}^2(N_2+1)]^2}\times(1-\cos\Omega_{2\gamma}t_{int})\right]\ . \tag{3.1}$$

In the semiclassical approximation, we neglect the spontaneous emission terms and the width of the photon number probability distribution (given by the diagonal elements of the field density matrix in the Fock-state representation). We expect these to be good approximations in the limit of large average photon numbers $\langle N_1\rangle$ and $\langle N_2\rangle$, which as we shall see corresponds to the limit

$$t_{cav_1}/t_{at},t_{cav_2}/t_{at}\gg 1\ .$$

In order to simplify the calculations, we assume that

$$\Omega_{ei}=\Omega_{if}=g\ .$$

The results for $\Omega_{ei}\neq\Omega_{if}$ are qualitatively the same, and are discussed in Appendix B. From Eq. (3.1), we get, in this limit,

$$G=\frac{1}{t_{at}}\frac{4\bar{N}_1\bar{N}_2}{(\bar{N}_1+\bar{N}_2)^2}\sin^2[g^2(\bar{N}_1+\bar{N}_2)t_{int}/2\Delta]\ , \tag{3.2}$$

where $\bar{N}_1$ and $\bar{N}_2$ are the mean photon numbers.

Assuming now that the cavity dissipation and the atomic gain are completely independent processes, which should be true if $t_{int}\ll t_{cav_i}$, we get the following rate equations for the photon numbers in the two modes:

$$\frac{d\bar{N}_1}{dt}=\frac{1}{t_{at}}\frac{4\bar{N}_1\bar{N}_2}{(\bar{N}_1+\bar{N}_2)^2}\times\sin^2[g^2(\bar{N}_1+\bar{N}_2)t_{int}/2\Delta]-\frac{\bar{N}_1}{t_{cav_1}}\ , \tag{3.3a}$$

$$\frac{d\bar{N}_2}{dt}=\frac{1}{t_{at}}\frac{4\bar{N}_1\bar{N}_2}{(\bar{N}_1+\bar{N}_2)^2}\times\sin^2[g^2(\bar{N}_1+\bar{N}_2)t_{int}/2\Delta]-\frac{\bar{N}_2}{t_{cav_2}}\ . \tag{3.3b}$$

Following Ref. 5, we define the renormalized mean photon numbers:

$$n_1=\bar{N}_1 t_{at}/t_{cav_1},\quad n_2=\bar{N}_2 t_{at}/t_{cav_1},$$

so that

$$\frac{dn_1}{dt}=\frac{1}{t_{cav_1}}\frac{4n_1n_2}{(n_1+n_2)^2}\sin^2\alpha(n_1+n_2)-\frac{n_1}{t_{cav_1}}, \tag{3.4a}$$

$$\frac{dn_2}{dt}=\frac{1}{t_{cav_1}}\frac{4n_1n_2}{(n_1+n_2)^2}\sin^2\alpha(n_1+n_2)-\frac{n_2}{t_{cav_2}}, \tag{3.4b}$$

where

$$\alpha=\frac{g^2 t_{int}t_{cav_1}}{2\Delta t_{at}}. \tag{3.5}$$

The steady-state solutions are obtained by setting $dn_1/dt=dn_2/dt=0$. Since the gains for the two modes are equal, the steady-state values must obey the relation

$$\frac{n_1}{t_{cav_1}}=\frac{n_2}{t_{cav_2}}, \tag{3.6}$$

implying that the steady-state values of n_1 are given by the roots of

$$n_1=\frac{4t_{cav_1}t_{cav_2}}{(t_{cav_1}+t_{cav_2})^2}\sin^2\left[\alpha n_1\frac{(t_{cav_1}+t_{cav_2})}{t_{cav_1}}\right]. \tag{3.7}$$

This equation may be solved graphically, as sketched in Fig. 4. The graphical analysis may also provide information about the stability of the steady-state solutions when n_1 and n_2 are related by Eq. (3.6). It does not assure, however, the global stability in the two-dimensional $n_1\times n_2$ plane. In order to check this point, we linearize the coupled equations (3.4) around the steady-state values. The detailed procedure is discussed in Appendix B, in the general situation where $\Omega_{ei}\neq\Omega_{if}$. The main conclusion is that points which are stable under condition (3.6) remain so when that relation is violated. In particular, the zero-field point is always stable, as in the degenerate case. The system becomes therefore bistable, immediately above threshold. For sufficiently low dissipation, other stable points may appear. As shown in Appendix B, the approach to steady state may be oscillatory when $t_{cav_1}\neq t_{cav_2}$. This will happen when the slope of the gain curve at the steady-state point is in an interval with a width $(t_{cav_1}-t_{cav_2})^2/2t_{cav_1}t_{cav_2}$, which increases as

$$\frac{|t_{cav_1}-t_{cav_2}|}{t_{cav_1}+t_{cav_2}}\to 1, \tag{3.8}$$

that is, when the two damping times become quite different from each other. The oscillations are typically strongly damped, except in the limit given by Eq. (3.8).

The semiclassical analysis yields the threshold condition: it is given by the first nonzero solution of Eq. (3.7), as shown in Fig. 4(a). We notice that when the damping times are very different [as in Eq. (3.8)], it becomes more difficult to reach the threshold, since the amplitude of the gain term may be written as [see Eq. (3.7)]

$$\frac{4t_{cav_1}t_{cav_2}}{(t_{cav_1}+t_{cav_2})^2}=1-\frac{(t_{cav_1}-t_{cav_2})^2}{(t_{cav_1}+t_{cav_2})^2}.$$

This result can be easily interpreted in terms of the effect discussed at the end of Sec. II: in the limit given by Eq. (3.8), the steady-state mean photon numbers become very different, as shown by Eq. (3.6), so that the Stark shift induces a large effective detuning, thus lowering the atomic gain.

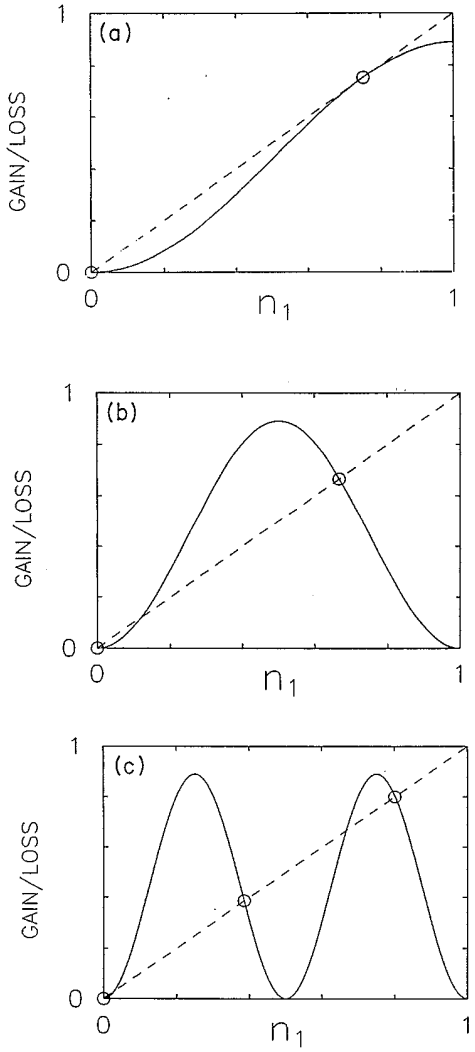

FIG. 4. Semiclassical model of the nondegenerate two-photon micromaser in the large-detuning limit: gain and loss contributions to $\bar{n}_1$ vs $\bar{n}_1$, where $\bar{n}_1$ is the normalized photon number in the upper mode. The loss term is proportional to $\bar{n}_1$ (dashed line). The three curves correspond to $t_{cav_1}=2t_{cav_2}$, and to (a) $\alpha=1{,}03$; (b) $\alpha=\pi/3$; (c) $\alpha=2\pi/3$. Stable operation points are shown by circles. The system is at the threshold of oscillation in curve (a). (c) displays three stable operation points for a larger value of the normalized pump α.

Even if $t_{cav_1}=t_{cav_2}$, the threshold is higher than in the degenerate case. In this case, the threshold may be estimated by noticing, from Eq. (3.6), that we must have equal intensities in the two modes ($n_1=n_2=n$), and by setting $n=1$ and the Rabi angle $g^2 t_{int} t_{cav_1} n/\Delta t_{at}$ equal to $\pi/2$, where the gain is maximum, so that

$$\left.\frac{1}{t_{at}}\right|_{threshold} \simeq \frac{\pi\Delta}{2g^2 t_{int} t_{cav_1}} , \tag{3.9}$$

which is two times larger than the value for the degenerate case.[4,5] A similar discrepancy has been found for the two-photon laser;[15] there is no paradox here, since, due to condition (1.1), one cannot go continuously from our model to the one corresponding to the degenerate micromaser.

When $\Omega_{ei}\neq\Omega_{if}$, the results are very similar (Appendix B). The only difference is that the condition for the oscillation regime is now

$$\left[\frac{\Omega_{t_>}}{\Omega_{t_<}}\right]^4 > \frac{t_<}{t_>} ,$$

where $t_>$ ($t_<$) is the largest (smallest) damping time and $\Omega_{t_>}$ ($\Omega_{t_<}$) the corresponding coupling ($\Omega_{t_{cav_1}}=\Omega_{ei}$, $\Omega_{t_{cav_2}}=\Omega_{if}$).

(b) Zero detuning: $\Delta=0$. As in the large-detuning case, the semiclassical rate equations contain the cavity loss terms—which are the same as before—and the atomic gain for each mode, given by Eqs. (2.14) and (2.15). When

$$\Omega_{ei}=\Omega_{if}=g ,$$

the transition probabilities $e\rightarrow i$ and $e\rightarrow f$ are given, respectively, by

$$|b(\bar{N}_1,\bar{N}_2,t_{int})|^2=\frac{\bar{N}_1}{\bar{N}_1+\bar{N}_2}\sin^2 g\sqrt{\bar{N}_1+\bar{N}_2}\,t_{int} , \tag{3.10}$$

$$|c(\bar{N}_1,\bar{N}_2,t_{int})|^2=\frac{4\bar{N}_1\bar{N}_2}{(\bar{N}_1+\bar{N}_2)^2}\sin^4\frac{g\sqrt{\bar{N}_1+\bar{N}_2}\,t_{int}}{2} , \tag{3.11}$$

and then the semiclassical equations are

$$\frac{d\bar{N}_1}{dt}=\frac{1}{t_{at}}\left[\frac{\bar{N}_1}{\bar{N}_1+\bar{N}_2}\sin^2 g\sqrt{\bar{N}_1+\bar{N}_2}\,t_{int}+\frac{4\bar{N}_1\bar{N}_2}{(\bar{N}_1+\bar{N}_2)^2}\sin^4\frac{g\sqrt{\bar{N}_1+\bar{N}_2}\,t_{int}}{2}\right]-\frac{\bar{N}_1}{t_{cav_1}} , \tag{3.12}$$

$$\frac{d\bar{N}_2}{dt}=\frac{1}{t_{at}}\frac{4\bar{N}_1\bar{N}_2}{(\bar{N}_1+\bar{N}_2)^2}\times\sin^4\frac{g\sqrt{\bar{N}_1+\bar{N}_2}\,t_{int}}{2}-\frac{\bar{N}_2}{t_{cav_2}} . \tag{3.13}$$

As in the laser case,[14] we have in general a different threshold condition for each mode. Unless $t_{cav_2}\gg t_{cav_1}$, the threshold for the lower mode will be obviously higher. Therefore, the lower mode steady-state intensity $\bar{N}_2$ will be zero near the threshold of the upper mode, where Eq. (3.12) gets

$$\frac{d\bar{N}_1}{dt}=\frac{1}{t_{at}}\sin^2 g\sqrt{\bar{N}_1}\,t_{int}-\frac{\bar{N}_1}{t_{cav_1}} , \tag{3.14}$$

which is exactly the semiclassical one-photon-micromaser equation.[3] Since the $|i\rangle\leftrightarrow|f\rangle$ transition is semiclassically frozen below the threshold of oscillation of the lower mode, our system behaves as the usual one-photon micromaser for low pump parameters.

In particular, the threshold for the upper mode is given by[3]

$$\theta\equiv g t_{int}\left[\frac{t_{cav_1}}{t_{at}}\right]^{1/2}>1 . \tag{3.15}$$

The threshold for the lower mode is obtained in Appendix D when the cavity damping times are equal,

$$t_{cav_1}=t_{cav_2}=t_{cav} ,$$

which is assumed from now on. We prove that a steady-state oscillations in the lower mode ($\bar{N}_2\neq0$) is reached only for

$$\theta>\pi/2 .$$

Besides, we show in Appendix C that the one-mode solution

$$\bar{N}_1=\frac{t_{cav}}{t_{at}}\sin^2 g\sqrt{\bar{N}_1}\,t_{int} , \tag{3.16a}$$

$$\bar{N}_2=0 \tag{3.16b}$$

becomes unstable above this threshold. As in the one-photon micromaser, we have a continuous "phase transition" here: $\bar{N}_2$ grows up continuously from the zero value at threshold. However, the behavior for larger values of the pump θ is quite unusual, because the one-mode solution given by Eqs. (3.16) gets stable again if

$$-\pi/2\leq g t_{int}(\bar{N}_1^S)^{1/2}+2n\pi\leq\pi/2, \quad n\in Z \tag{3.17}$$

for some integral value of n (see Appendix C), where the superscript S stands for steady state. In Fig. 5 we show a one-mode solution at the point where it is getting stable again for the first time. It corresponds, from Eq. (3.17), to a Rabi angle given by

$$g\sqrt{\bar{N}_1}\,t_{int}=\frac{3\pi}{2} , \tag{3.18}$$

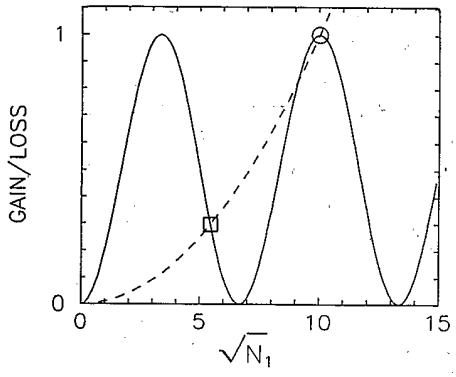

FIG. 5. Semiclassical model of the micromaser with zero detuning ($\Delta=0$): gain (solid line) and loss (dashed line) contributions to $\bar{N}_1$ vs $\sqrt{\bar{N}_1}$ when there is no oscillation in the lower mode. $\bar{N}_1$ is the mean number of photons in the upper mode. The parameters are $t_{cav}/t_{at}=100$, $gt_{int}=3\pi/20$, so that $\theta=3\pi/2$. One can see two stable solutions of the one-photon micromaser rate equation [Eq. (3.14)]. The point shown by a circle corresponds to a stable operation point of the two-photon micromaser, whereas the one shown by a square corresponds to an unstable one-mode steady-state solution of the two-photon micromaser rate equations [Eqs. (3.12) and (3.13)]. Note that the vacuum is always unstable above the threshold of the upper mode.

and, from Eq. (3.16a), to an intensity given by

$$\bar{N}_1=\frac{t_{cav}}{t_{at}}\ , \tag{3.19}$$

which is the maximum possible value. From Eqs. (3.15), (3.18), and (3.19), the pump is, in this case,

$$\theta=\frac{3\pi}{2}\ .$$

Meanwhile, the other solution of Eq. (3.16a) for this pump value (shown in Fig. 5) does not get stable, for it corresponds to a smaller value of the Rabi angle (in the second quadrant).

More generally, we have a stable one-mode solution when the pump parameter θ is found in the intervals

$$-\frac{\pi}{2}\le\theta+2n\pi\le\frac{\pi}{2},\quad n\in Z\ . \tag{3.20}$$

When $\theta<\pi/2$, this solution is the only one: we are below the lower mode threshold.

As we increase the pump θ, a new stable one-mode solution shows up at the critical points

$$\theta=3\pi/2,7\pi/2,\ldots$$

given by the maximum allowed intensity

$$\bar{N}_1=t_{cav}/t_{at}\ .$$

However, the oscillation in the lower mode will *not* cease at these points. In order to operate the micromaser with $\bar{N}_2=0$ when θ satisfies Eq. (3.20) one must start from an operating point inside the basin of attraction of the stable solution given by Eq. (3.16). We summarize these results in Table I, showing the many different operation regimes as θ varies.

From Eqs. (3.12) and (3.13)—with $t_{cav_1}=t_{cav_2}$—we see that

$$\bar{N}_1^S\ge\bar{N}_2^S\ ,$$

and that the equality holds if and only if

$$g(\bar{N}_1^S+\bar{N}_2^S)^{1/2}t_{int}=n\pi,\quad n\in Z\ , \tag{3.21}$$

with

$$\bar{N}_2^S=\bar{N}_1^S=\frac{t_{cav}}{t_{at}}\sin^4(n\pi/2)=t_{cav}/t_{at}\ , \tag{3.22}$$

if n is odd. If n is even, we get just the trivial (and unstable) solution $\bar{N}_1=\bar{N}_2=0$.

We have therefore

$$\theta=\frac{n\pi}{\sqrt{2}},\quad n\ \text{odd}\ , \tag{3.23}$$

as the condition for having an equal number of photons in the two modes at steady state. In this case, the atom is never found in the intermediate state when leaving the cavity, so that a genuine two-photon process takes place, even though the intermediate state is exactly tuned to resonance.

In order to get a better physical insight into this situation, we plot in Fig. 6 the transition probabilities for the $e\leftrightarrow i$ and $e\leftrightarrow f$ Rabi precessions [Eqs. (3.10) and (3.11), respectively] as functions of the Rabi precession angle

$$\theta_R(\bar{N}_1^S,\bar{N}_2^S)=g(\bar{N}_1^S+\bar{N}_2^S)^{1/2}t_{int}\ .$$

We normalize the two amplitudes of oscillation to one. The odd n values in Eq. (3.21) correspond to the situation

TABLE I. Semiclassical model of the micromaser with zero detuning: summary of the results for the threshold of oscillation and the stability of the vacuum field. θ is the generalized pump defined by Eq. (3.15).

θ	0	1	$\pi/2$	$3\pi/2$	$5\pi/2$	$7\pi/2$
Upper mode	below threshold	above threshold $n_1=0$ unstable				
Lower mode	below threshold		$n_2=0$ unstable	above threshold $n_2=0$ stable		$n_2=0$ unstable

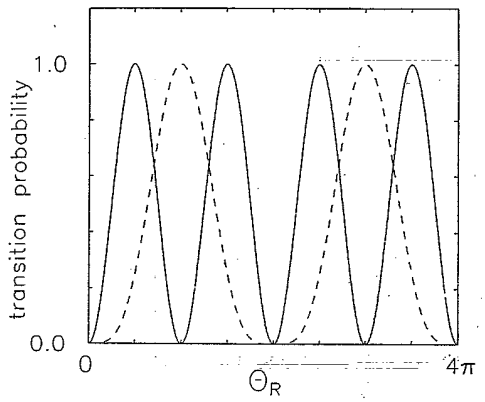

FIG. 6. Semiclassical model in the zero-detuning case: Rabi precessions for the $e\leftrightarrow i$ (solid line) and $e\leftrightarrow f$ (dashed line) transitions as a function of the Rabi angle $\theta_R(\bar{N}_1,\bar{N}_2)$. Note that the maximum values of the $e\leftrightarrow f$ precession correspond to a zero $e\leftrightarrow i$ transition probability.

where the $e\leftrightarrow i$ Rabi vector makes a net complete revolution (zero transition probability) while the $e\leftrightarrow f$ Rabi vector just flips down (maximum transition probability).

In Appendix E we show that the steady state given by Eq. (3.22) is stable: we can achieve a "two-photon" operation regime even with zero detuning. This is a new and interesting possibility in two-photon micromaser physics, since in this case the condition of large detuning is relaxed, opening the possibility of oscillation with a larger number of photons [see Eq. (2.16)].

These results depend very strongly on the monokinetic character of the atomic beam. In the limit of a broad velocity distribution, the micromaser becomes identical to a two-photon nondegenerate laser. Then, the upper mode intensity is always larger than the lower one, and there exist at most two stable operating points.[14]

The analysis made in this section has allowed the discussion of some of the interesting features of the nondegenerate two-photon micromaser: we have evaluated the oscillation threshold in many different situations, and we have shown that the system may become multistable. The operating points can be obtained graphically, as sketched in Fig. 4. The zero-field point, according to this semiclassical analysis, is always stable in the large-detuning limit, but becomes unstable for zero detuning. Of course, for low photon numbers, quantum effects should play an important role. They will be discussed in the next section in the large-detuning limit. In a forthcoming paper, we plan to discuss the quantum theory in the resonant case.

IV. QUANTUM THEORY

A. Master equation

It has been shown[3,5,16] that the master equation for the field density operator ρ has a simpler form when the incoming excited atoms have a Poissonian distribution of the arrival times—besides, this is the most common experimental situation. We also assume that, with $t_{\rm cav} \gg t_{\rm int}$, gain and dissipation are independent processes, since they act on very different time scales. Then, following Refs. 3–5 and 17, we may write

$$\frac{d\rho}{dt}=\frac{d\rho}{dt}\bigg|_{\substack{\text{atomic}\\ \text{gain}}}+L\rho \ ,$$

where

$$L\rho=\sum_{i=1,2}\frac{1}{2t_{\text{cav}_i}}(2a_i\rho a_i^{\dagger}-a_i^{\dagger}a_i\rho-\rho a_i^{\dagger}a_i)$$

is the usual term associated with cavity dissipation at zero temperature.

In the Fock-state representation, the gain terms are given by

$$\begin{aligned}\frac{d}{dt}\rho_{N_1N_2;M_1M_2}\bigg|_{\substack{\text{atomic}\\ \text{gain}}}=\frac{1}{t_{\text{at}}}\{&-[1-a(N_1,N_2,t_{\text{int}})a^*(M_1,M_2,t_{\text{int}})]\rho_{N_1N_2;M_1M_2}\\ &+c(N_1,N_2,t_{\text{int}})c^*(M_1,M_2,t_{\text{int}})\rho_{N_1-1,N_2-1;M_1-1,M_2-1}\\ &+b(N_1,N_2,t_{\text{int}})b^*(M_1,M_2,t_{\text{int}})\rho_{N_1-1,N_2;M_1-1,M_2}\}\ ,\end{aligned} \tag{4.1}$$

where

$$\rho_{N_1N_2;M_1M_2}=\langle N_1N_2|\rho|M_1M_2\rangle \ ,$$

and a,b, and c are the coefficients defined by Eqs. (2.11)–(2.13) and (A4). The diagonal elements $\rho_{N_1N_2;N_1N_2}$ constitute the photon-number probability distribution:

$$\rho_{N_1N_2;N_1N_2}=\Pi_{N_1N_2}\geq 0 \ .$$

From Eq. (4.1), the master equation for $\Pi_{N_1N_2}$ is

$$\Pi_{N_1N_2}=-\frac{1}{t_{at}}\{[|b(N_1+1,N_2,t_{int})|^2+|c(N_1+1,N_2+1,t_{int})|^2]\Pi_{N_1N_2}$$
$$-|b(N_1,N_2,t_{int})|^2\Pi_{N_1-1,N_2}-|c(N_1,N_2,t_{int})|^2\Pi_{N_1-1,N_2-1}\}$$
$$-\left[\frac{N_1}{t_{cav_1}}+\frac{N_2}{t_{cav_2}}\right]\Pi_{N_1N_2}+\frac{N_1+1}{t_{cav_1}}\Pi_{N_1+1,N_2}+\frac{N_2+1}{t_{cav_2}}\Pi_{N_1,N_2+1}\,. \tag{4.2}$$

Although it is not possible to find a simple analytical form for the steady-state solution of Eq. (4.2), one may still get some useful results from this equation. Thus, we will analyze the phenomenon of spontaneous self-starting in Sec. IV B, while in Sec. IV C we obtain analytical results concerning the fluctuations in the difference of intensities of the two modes. In Sec. IV D we discuss the numerical solution of Eq. (4.2).

B. Spontaneous self-starting

As seen in Sec. III, in the two-photon micromaser the vacuum is classically stable in the limit of large detuning, meaning that it would be necessary for a triggering field in order to start maser action, even if one is above the oscillation threshold. Of course, in the low-intensity region, the classical approximation should be a poor one, and one expects quantum effects to play an important role. Indeed, as we will show in Sec. IV D, fluctuations associated with spontaneous emission render the vacuum state metastable, so that the maser actually starts oscillating after some time, even without a triggering field. Furthermore, as we show here, the vacuum may even become unstable, above a critical value of the pumping, implying a very fast start of the oscillation in a time of the order of t_{cav}. In analogy with the degenerate case,[5] we say that the vacuum becomes unstable when the steady-state photon-number probability distribution ceases to have a local maximum at the origin ($N_1=N_2=0$). One must have therefore $\Pi_{00}<\Pi_{10}$ or Π_{01} at steady state.

The precise conditions for this to happen may be found from the master equation (4.2), with $N_1=N_2=0$:

$$\dot{\Pi}_{00}=-\frac{1}{t_{at}}[|b(1,0,t_{int})|^2+|c(1,1,t_{int})|^2]\Pi_{00}$$
$$+\frac{\Pi_{10}}{t_{cav_1}}+\frac{\Pi_{01}}{t_{cav_2}}\,. \tag{4.3}$$

For simplicity, we analyze this equation in the case of equal damping times, $t_{cav_1}=t_{cav_2}=t_{cav}$, equal couplings, $\Omega_{ei}=\Omega_{if}=g$, and in the limit of large detuning. In this limit, the master equation becomes symmetric upon interchange of N_1 and N_2, and the steady-state probability distribution satisfies

$$\Pi^S_{N_1N_2}=\Pi^S_{N_2N_1}\,, \tag{4.4}$$

so that the instability condition becomes

$$\Pi^S_{00}<\Pi^S_{10}=\Pi^S_{01}\,, \tag{4.5}$$

where the superscript S stands as before for "steady-state." From Eqs. (4.3) and (4.5), we get

$$\frac{1}{t_{at}}[|b(1,0,t_{int})|^2+|c(1,1,t_{int})|^2]>\frac{2}{t_{cav}}\,, \tag{4.6}$$

which has a simple physical interpretation: the vacuum becomes unstable when the total rate of spontaneous emission into the two modes, represented by the left-hand side of Eq. (4.6), gets larger than the total dissipation rate.

Typical experimental values[2] imply a small two-photon spontaneous emission Rabi angle $g^2t_{int}/\Delta\ll1$, so that Eq. (4.6) may be approximated by

$$\frac{1}{t_{at}}\{4(g/\Delta)^2\sin^2(\Delta t_{int}/2)$$
$$+(g^2t_{int}/\Delta)^2+O[(g^2t_{int}/\Delta)^4]\}>\frac{2}{t_{cav}}\,. \tag{4.7}$$

Furthermore, since typically $gt_{int}\simeq10$, the first term on the left-hand side of Eq. (4.7)—which comes from the one-photon correction to the two-photon transition—is approximately 10^{-2} smaller than the second term. Thus, from (3.5), we finally get the condition

$$\alpha^2>\frac{1}{2}\frac{t_{cav}}{t_{at}} \tag{4.8}$$

for the vacuum to become unstable (spontaneous self-starting). Equation (4.8) has a form similar to the one for the degenerate micromaser, except for the fact that the pumping should be approximately two times larger here, as in the comparison between the thresholds in the degenerate and nondegenerate cases of Sec. III. When the condition of large gt_{int} is not met, the first term on the left-hand side of Eq. (4.7), associated with the one-photon cascade process, can, in principle, change the stability of the origin. Then, larger values of α would be necessary in order to reach the threshold condition.

Finally, we note that the real (quantum) threshold of the system is somewhere in between the classical condition (3.9) and the instability threshold [Eq. (4.8)]. As the pumping decreases from the limit value given by Eq. (4.8) in the direction of the quantum threshold, the self-starting time grows exponentially with t_{cav}/t_{at} (cf. Ref. 5). The vacuum becomes stable as $t_{cav}/t_{at}\to\infty$, which corresponds to the semiclassical limit.

C. Quantum fluctuations

As we noted in the introduction, the nondegenerate micromaser is a very interesting system in the limit of large

detuning because the gain process feeds the field intensities of both modes without introducing noise in their difference. More precisely, we start from the master equation (4.2) in the limit

$$\Delta^2 \gg \Omega_{ei}^2 N_1, \Omega_{if}^2 N_2 ,$$

where the "one-photon" contribution bb^* goes to zero (see Sec. II). Then we get

$$\dot{\Pi}_{N_1,N_2} = -G(N_1+1,N_2+1)\Pi_{N_1,N_2} + G(N_1,N_2)\Pi_{N_1-1,N_2-1} - \frac{N_1}{t_{\mathrm{cav}_1}}\Pi_{N_1N_2} - \frac{N_2}{t_{\mathrm{cav}_2}}\Pi_{N_1N_2} + \frac{(N_1+1)\Pi_{N_1+1,N_2}}{t_{\mathrm{cav}_1}} + \frac{(N_2+1)\Pi_{N_1,N_2+1}}{t_{\mathrm{cav}_2}} , \tag{4.9}$$

where

$$G(N_1,N_2) = c(N_1,N_2,t_{\mathrm{int}})c^*(N_1,N_2,t_{\mathrm{int}})/t_{\mathrm{at}}$$

is the two-photon gain rate. From Eq. (4.9), we get

$$\frac{d}{dt}\langle N_1 - N_2\rangle = -\sum_{N_1N_2}(N_1-N_2)G(N_1+1,N_2+1)\Pi_{N_1N_2} + \sum_{N_1N_2}(N_1-N_2)G(N_1,N_2)\Pi_{N_1-1,N_2-1} + \sum_{N_1N_2}(N_1-N_2)\left[-\left[\frac{N_1}{t_{\mathrm{cav}_1}}+\frac{N_2}{t_{\mathrm{cav}_2}}\right]\Pi_{N_1N_2} + \frac{(N_1+1)}{t_{\mathrm{cav}_1}}\Pi_{N_1+1,N_2} + \frac{(N_2+1)}{t_{\mathrm{cav}_2}}\Pi_{N_1,N_2+1}\right]$$

and

$$\frac{d}{dt}\langle (N_1-N_2)^2\rangle = -\sum_{N_1N_2}(N_1-N_2)^2G(N_1+1,N_2+1)\Pi_{N_1N_2} + \sum_{N_1N_2}(N_1-N_2)^2G(N_1,N_2)\Pi_{N_1-1,N_2-1} + \sum_{N_1N_2}(N_1-N_2)^2\left[-\left[\frac{N_1}{t_{\mathrm{cav}_1}}+\frac{N_2}{t_{\mathrm{cav}_2}}\right]\Pi_{N_1N_2} + \frac{(N_1+1)}{t_{\mathrm{cav}_1}}\Pi_{N_1+1,N_2} + \frac{(N_2+1)}{t_{\mathrm{cav}_2}}\Pi_{N_1,N_2+1}\right] .$$

In both equations the gain terms cancel out, and then

$$\frac{d}{dt}\langle N_1 - N_2\rangle = -\frac{\langle N_1\rangle}{t_{\mathrm{cav}_1}} + \frac{\langle N_2\rangle}{t_{\mathrm{cav}_2}} , \tag{4.10}$$

which is hardly a surprising result. On the other hand,

$$\frac{d}{dt}\langle (N_1-N_2)^2\rangle = \frac{\langle N_1\rangle}{t_{\mathrm{cav}_1}} + \frac{\langle N_2\rangle}{t_{\mathrm{cav}_2}} - \frac{2\langle N_1(N_1-N_2)\rangle}{t_{\mathrm{cav}_1}} + \frac{2\langle N_2(N_1-N_2)\rangle}{t_{\mathrm{cav}_2}} , \tag{4.11}$$

which shows that all the noise in the difference of intensities comes from cavity dissipation, which removes photons from the beams randomly, acting independently for each mode.

From now on, we explore the particular case

$$t_{\mathrm{cav}_1} = t_{\mathrm{cav}_2} = t_{\mathrm{cav}} , \tag{4.12}$$

which exhibits in a simple way the nonclassical features of the nondegenerate micromaser. At steady state, we get from Eqs. (4.10)–(4.12)

$$\langle N_i\rangle = \langle N_2\rangle$$

and

$$\langle (N_1-N_2)^2\rangle = \frac{\langle N_1+N_2\rangle}{2} . \tag{4.13}$$

On the other hand, for a classical field distribution, we must have[18]

$$\langle (N_1-N_2)^2\rangle - \langle N_1-N_2\rangle^2 \geq \langle N_1+N_2\rangle .$$

Therefore, we have a squeezing factor of 50% for the intracavity field. The important point here is that this result is explicitly independent of the gain process, so that we have a general result that applies equally well to all kinds of two-photon nondegenerate oscillators, as for instance the two-photon laser. Violations of classical inequalities were also sought by Zubairy for a two-photon laser far above threshold.[19] For the correlation functions considered by him, only small effects could be found. We see now that the squeezing in the difference of intensities may reach 50%, at steady state, either above or below the threshold.

D. Numerical results

Since we cannot obtain a simple analytical expression for the steady-state density operator (because of the higher dimensionality of the problem), the numerical approach becomes indispensable. We present here the time evolution of the diagonal elements of the density operator in three different regimes: (i) below the threshold of oscillation, (ii) above the threshold of oscillation, but below

the self-starting threshold, and (iii) above the self-starting threshold. We use numerical values typical of the degenerate micromaser.[4]

$$t_{\mathrm{cav}_1}=t_{\mathrm{cav}_2}=0.4\ \mathrm{ms}\ ,$$
$$\Omega_{ei}=7.3\times10^5\ \mathrm{s}^{-1}\ ,$$
$$\Omega_{if}=7.5\times10^5\ \mathrm{s}^{-1}\ , \tag{4.14}$$
$$\frac{\Delta}{2\pi}=39\times10^6\ \mathrm{s}^{-1}\ ,$$
$$t_{\mathrm{int}}=2.5\times10^{-5}\ \mathrm{s}\ .$$

Then

$$\frac{\Omega_{ei}^2}{\Delta^2},\frac{\Omega_{if}^2}{\Delta^2}\sim10^{-5}\ ,$$

and since the larger values of $\bar{N}_1$, $\bar{N}_2$ are at least of the order of $t_{\mathrm{cav}}/t_{\mathrm{at}}$, we have, for typical values of t_{at},

$$\bar{N}_1,\bar{N}_2\lesssim100\ ,$$
$$\frac{\Omega_{ei}^2}{\Delta^2}\bar{N}_1,\frac{\Omega_{if}^2}{\Delta^2}\bar{N}_2\lesssim10^{-3}\ .$$

Therefore, we are in the large-detuning limit, and the master equation is (4.9) with $t_{\mathrm{cav}_1}=t_{\mathrm{cav}_2}$. The different regimes are defined by the different values of the pumping t_{at}^{-1}.

(i) $t_{\mathrm{at}}^{-1}=10^5\ \mathrm{s}^{-1}$. From Eq. (3.9) we see that we are above the classical threshold, since

$$\frac{\pi}{g^2t_{\mathrm{int}}t_{\mathrm{cav}}}\frac{\Delta}{2}\sim7\times10^4\ \mathrm{s}^{-1}\ ,$$

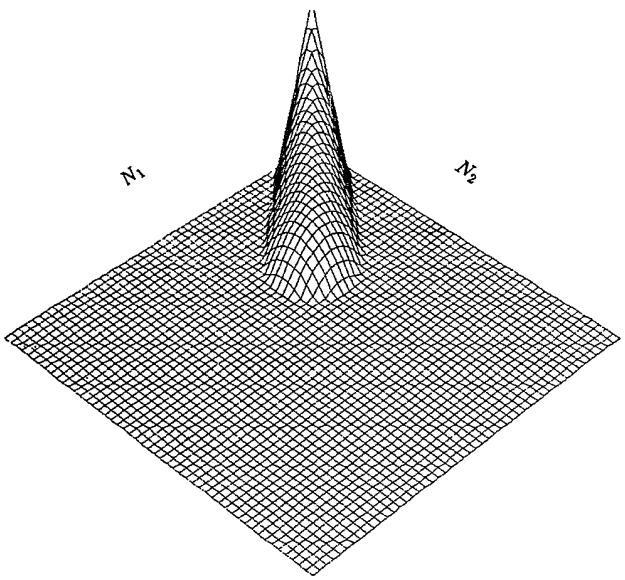

FIG. 7. Steady-state photon distribution in the limit of large detuning below the threshold of oscillation. The graph corresponds to $\alpha=1,1$ and $t_{\mathrm{at}}=10^{-5}$ s [see Eqs. (3.5) and (4.14)].

but Fig. 7 shows that we have no oscillation: the steady state is concentrated around the origin. We conclude that the real threshold condition is higher than the classical one.

(ii) $t_{\mathrm{at}}^{-1}=10^6\ \mathrm{s}^{-1}$. Then $t_{\mathrm{int}}\gg t_{\mathrm{at}}$, which seems to contradict our basic hypothesis of one-atom interaction. However, since the dynamics depends on t_{at} only through $t_{\mathrm{cav}}/t_{\mathrm{at}}$ [see Eq. (4.2)], we can associated with this case a larger t_{cav} and a smaller t_{at}^{-1}, with

$$t_{\mathrm{cav}}/t_{\mathrm{at}}=400$$

fixed, and $t_{\mathrm{at}}\gtrsim t_{\mathrm{int}}$. Of course, the time scale of the evolution would be completely changed.

Figure 8 shows the time evolution of the field probability distribution. We see that the starting time is finite, and of the order of $5t_{\mathrm{cav}}$, which means that the vacuum state is metastable. Figure 9 shows the steady state from different angles. The symmetry $\bar{N}_1\leftrightarrow\bar{N}_2$ is particularly evident in Fig. 9(b).

From Fig. 8, one sees that the variance $\langle(N_1-N_2)\rangle^2$ starts to increase at $t\simeq t_{\mathrm{cav}}$. Before that time, dissipation does not affect the field very much and the distribution is very concentrated around $\bar{N}_1=\bar{N}_2$. At $t\gtrsim t_{\mathrm{cav}}$, dissipation becomes important, and the fluctuation grows up, confirming our previous discussion about the role of dissipation, which randomly removes photons from both modes. In order to clarify this point, we plot in Fig. 10 the variance $\langle(N_1-N_2)^2\rangle$ against time. The sudden increase of the fluctuations at $t\simeq t_{\mathrm{cav}}$ becomes quite apparent.

Finally, we note that the steady-state averages $\langle N_1\rangle,\langle N_2\rangle$ are in good agreement with the classical ones, which are the roots of [cf. Eqs. (3.6) and (3.7), with $t_{\mathrm{cav}_1}=t_{\mathrm{cav}_2}$, and the values given by Eq. (4.14)]

$$\langle N_1\rangle=\langle N_2\rangle=400\sin^2(5.6\times10^{-2}\langle N_1\rangle)\ ,$$

given by

$$\langle N_1\rangle=\langle N_2\rangle\simeq50\ .$$

(iii) $t_{\mathrm{at}}^{-1}=3\times10^6\ \mathrm{s}^{-1}$. Figure 11 displays the distribution at $t=1$ ms (not yet the steady state), showing the quantum counterpart of the classical multistability. As the pumping rate goes up, the distribution is gradually removed from the first classical stable state, reminiscent of the one shown in Fig. 9, and peaks around the next classical solution: this is a diffusion process well known from the quantum theory of the degenerate micromaser. Now, the starting time is less than t_{cav}: the vacuum state becomes unstable. Indeed, the inequality (4.8) predicts that this would happen when

$$\frac{1}{t_{\mathrm{at}}}>1.4\times10^6\ \mathrm{s}^{-1}\ .$$

Therefore, we see that the numerical results in both regimes II and III agree well with our analytical work.

V. CONCLUSION

The main novelty of the nondegenerate two-photon micromaser, with respect to the degenerate one, is the strong correlation between the two modes, which may produce a 50% squeezing in the difference of intensities at steady state. Furthermore, the numerical integration of the master equation shows that, for small times ($t \ll t_{cav}$), the variance of the difference of intensities may be even smaller.

The semiclassical analysis led, on the other hand, to some other new features of the nondegenerate device, which are related to the threshold conditions for the two modes. Our treatment is based on a three-level model, and allows one to go continuously from the situation where the intermediate state is highly detuned to the resonant case. We have shown that, even in this case, it is still possible to have a genuine two-photon transition: for some values of the photon numbers, the intermediate state remains unpopulated.

In order to analyze the building up of the maser oscillation, one needs to take into account the quantum fluctuations. Starting from a three-level model, we get a master equation valid for any detuning. Therefore, it is possible to understand exactly how the two-photon transition regime is attained when the detuning is much larger than the two-photon Rabi frequency. We get the same result we would obtain through the effective two-level Hamiltonian approach of Refs. 4 and 5, which takes into account the Stark shifts of the upper and lower levels. This is in contrast with some recent results in the literature, showing that for two-photon *lasers* the effective Hamiltonian approach fails even in the region of large detunings.[13,14] Due to spontaneous decay, the in-

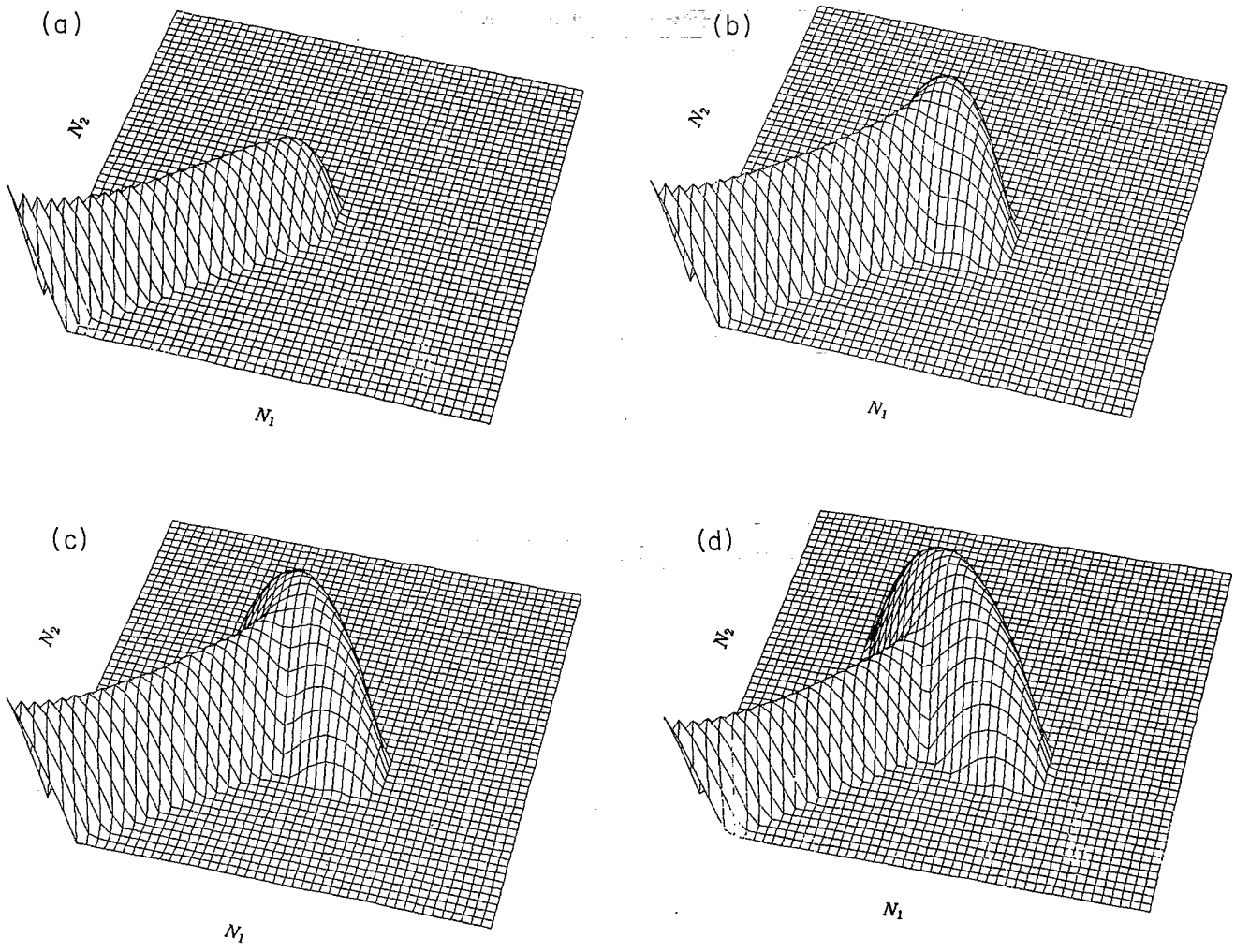

FIG. 8. Time evolution of the photon number distribution in the limit of large detuning above the threshold of oscillation. The parameters are $\alpha=11$ and $t_{at}=10^{-6}$ s. At $t=0$, the distribution is centered at the origin. We show the distribution at (a) $t=0.25t_{cav}$, (b) $t=0.75t_{cav}$, (c) $t=1.5t_{cav}$, and (d) $t=5t_{cav}$. Note that the distribution broadens for $t \geq t_{cav}$, as we expected.

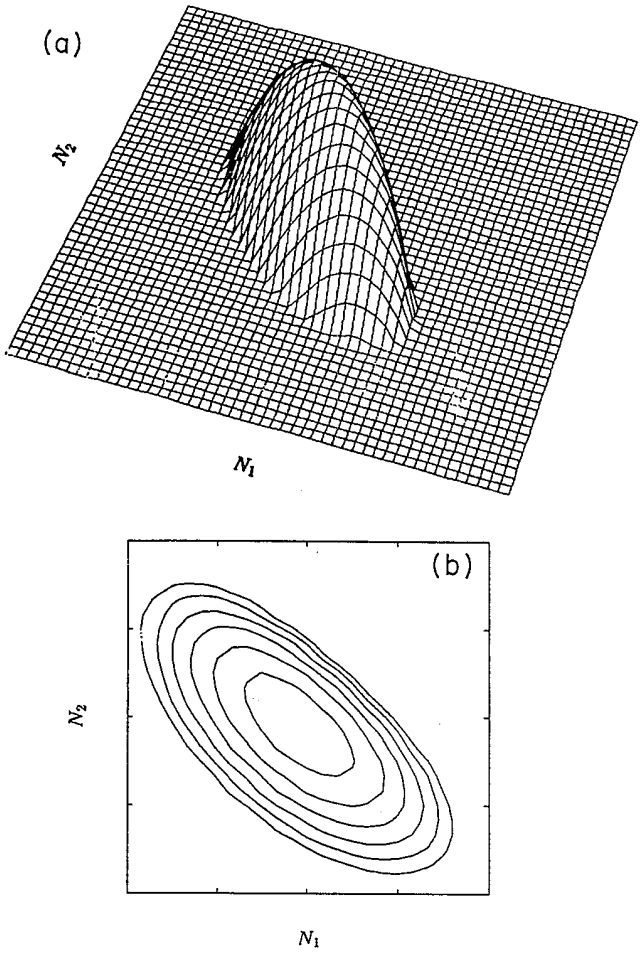

FIG. 9. Steady-state photon number distribution in the limit of large detuning above the threshold of oscillation, with the same parameters of Fig. 8. In (a), one sees the graph from the same angle of Fig. 8, whereas in (b) we plot the curve of π_{N_1,N_2} constant in the $N_1 \times N_2$ plane, showing the $N_1 \leftrightarrow N_2$ symmetry.

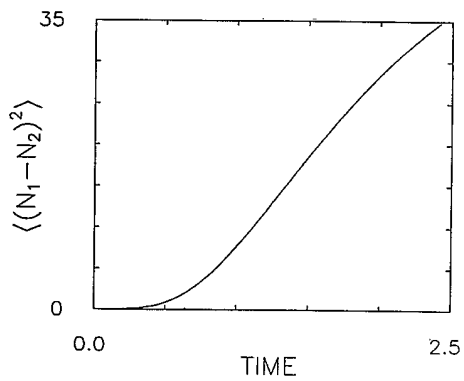

FIG. 10. Initial time evolution of the variance of the difference of intensities $\langle (N_1-N_2)^2 \rangle$. Time is expressed in units of t_{cav}. All the parameters are equal to those of Figs. 8 and 9. Note that the fluctuations begin to grow up for $t \gtrsim t_{cav}$. For $t \to \infty$, as expected, $\langle N_1-N_2)^2 \rangle \to (\langle N_1 \rangle + \langle N_2 \rangle)/2 = 42$.

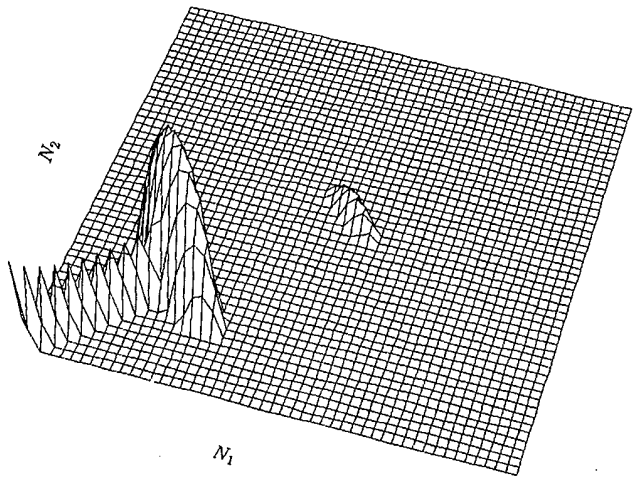

FIG. 11. Photon distribution in the limit of large detuning well above the threshold of oscillation, displaying the quantum counterpart of the classical multistability. The graph corresponds to $t = 2.5 t_{cav}$, with $\alpha = 33$. $t_{at} = \frac{1}{3} \times 10^{-6}$ s. The system is not yet in the steady state.

termediate level enlarges the laser linewidth by a factor of 2.

In our model, however, there is no spontaneous decay of the atomic levels. Then, the condition of small decay rate compared to the two-photon Rabi frequency—which, as the large detuning condition, should be satisfied in order to eliminate the intermediate level—holds automatically here. (We are grateful to Dr. S. Y. Zhu for discussions regarding this point.) Nevertheless, there remains the question: To what extent does the zero-decay approximation correspond to the real experimental conditions? Concerning this point, we note that in the degenerate micromaser experiment[2] the atomic levels had very large lifetimes, the one associated with the intermediate level being the largest one. Therefore, we can expect the consequences of the nonzero decays to be unimportant.

To conclude we should mention that the 50% squeezing [Eq. (4.14)] is a quite general result, valid whenever there is a true two-photon gain process—where the relay levels are not populated. A general discussion of this point is planned to be published elsewhere.

APPENDIX A: THE THREE-LEVEL- ATOM PROBLEM

We solve the Schrödinger equation

$$i\hbar \frac{\partial |\psi\rangle}{\partial t} = \overline{H}_{int} |\psi\rangle \ ,$$

where

$$\bar{H}_{\rm int}=\hbar\Omega_{ei}e^{-i\Delta t}a_1|e\rangle \times\langle i|+\hbar\Omega_{if}e^{i\Delta t}a_2|i\rangle\langle f|+\text{H.c.} \tag{A1}$$

for the three-level atom interacting with two modes of the electromagnetic field. The state $|\psi\rangle$ can be written as

$$|\psi\rangle=a(N_1,N_2,t)|e,N_1,N_2\rangle +b(N_1+1,N_2,t)|i,N_1+1,N_2\rangle +c(N_1+1,N_2+1,t)|f,N_1+1,N_2+1\rangle ,$$

so that Eq. (A1) yields

$$\begin{aligned} i\frac{\partial}{\partial t}a(N_1,N_2,t)&=\Omega_{ei}b(N_1+1,N_2,t)\sqrt{N_1+1}e^{-i\Delta t},\\ i\frac{\partial}{\partial t}b(N_1+1,N_2,t)&=\Omega_{if}c(N_1+1,N_2+1,t)\sqrt{N_2+1}e^{i\Delta t}+\Omega_{ei}a(N_1,N_2,t)\sqrt{N_1+1}e^{i\Delta t},\\ i\frac{\partial}{\partial t}c(N_1+1,N_2+1,t)&=\Omega_{if}b(N_1+1,N_2,t)\sqrt{N_2+1}e^{-i\Delta t}. \end{aligned} \tag{A2}$$

The Laplace transforms of these equations, with the initial conditions $a(0)=1$, $b(0)=c(0)=0$ are

$$\begin{aligned} &i[z\tilde{a}(z)-1]=\Omega_{ei}\sqrt{N_1+1}\tilde{b}(z+i\Delta),\\ &iz\tilde{b}(z)=\Omega_{if}\sqrt{N_2+1}\tilde{c}(z-i\Delta)+\Omega_{ei}\sqrt{N_1+1}\tilde{a}(z-i\Delta),\\ &iz\tilde{c}(z)=\Omega_{if}\sqrt{N_2+1}\tilde{b}(z+i\Delta). \end{aligned}$$

Solving for the Laplace transformed amplitudes $\tilde{a}$, $\tilde{b}$, and $\tilde{c}$, we get

$$\begin{aligned} \tilde{a}(z)&=\frac{1}{z}-\frac{\Omega_{ei}^2(N_1+1)}{z\left[z+\frac{i\Delta}{2}-i\Omega\right]\left[z+\frac{i\Delta}{2}+i\Omega\right]},\\ \tilde{b}(z)&=\frac{-i\Omega_{ei}\sqrt{N_1+1}}{\left[z-\frac{i\Delta}{2}-i\Omega\right]\left[z-\frac{i\Delta}{2}+i\Omega\right]},\\ \tilde{c}(z)&=\frac{-\Omega_{ei}\sqrt{N_1+1}\Omega_{if}\sqrt{N_2+1}}{z\left[z+\frac{i\Delta}{2}-i\Omega\right]\left[z+\frac{i\Delta}{2}+i\Omega\right]}, \end{aligned} \tag{A3}$$

where

$$\Omega=(\Omega_{ei}^2(N_1+1)+\Omega_{if}^2(N_2+1)+\Delta^2/4)^{1/2}.$$

The inverse Laplace transforms of Eqs. (A3) yield, finally, Eqs. (2.11) and (2.12), as well as the corresponding equation for $a(N_1,N_2,t)$, which should of course satisfy

$$|a(N_1,N_2,t)|^2=1-|b(N_1+1,N_2,t)|^2-|c(N_1+1,N_2+1,t)|^2. \tag{A4}$$

APPENDIX B: STABILITY ANALYSIS IN THE SEMICLASSICAL THEORY

We consider here the semiclassical theory in the more general situation in which $\Omega_{ei}\neq\Omega_{if}$. We write the semiclassical equations for the new variables

$$\xi_1=\frac{N_1\Omega_{ei}^2t_{\rm at}}{t_{\rm cav_1}},\quad \xi_2=\frac{N_2\Omega_{if}^2t_{\rm at}}{t_{\rm cav_1}},$$

and we define

$$\beta=\frac{t_{\rm cav_1}}{t_{\rm at}}\frac{t_{\rm int}}{\Delta},$$

so that the equations corresponding to (3.3) are written in the following way:

$$\begin{aligned} \frac{d\xi_1}{dt}&=-\frac{\xi_1}{t_{\rm cav_1}}+\frac{\Omega_{ei}^2}{t_{\rm cav_1}}\frac{2\xi_1\xi_2}{(\xi_1+\xi_2)^2}[1-\cos\beta(\xi_1+\xi_2)],\\ \frac{d\xi_2}{dt}&=-\frac{\xi_2}{t_{\rm cav_2}}+\frac{\Omega_{if}^2}{t_{\rm cav_1}}\frac{2\xi_1\xi_2}{(\xi_1+\xi_2)^2}[1-\cos\beta(\xi_1+\xi_2)]. \end{aligned} \tag{B1}$$

The steady-state values ξ_1^S and ξ_2^S must obey the relation [cf. Eq. (3.6)]

$$\frac{\xi_1^S}{\Omega_{ei}^2t_{\rm cav_1}}=\frac{\xi_2^S}{\Omega_{if}^2t_{\rm cav_2}}. \tag{B2}$$

We linearize now Eqs. (B1) around ξ_1^S, ξ_2^S. We set

$$\xi_1=\xi_1^S+e^{\lambda t}\Delta\xi_1,\quad \xi_2=\xi_2^2+e^{\lambda t}\Delta\xi_2,$$

and we expand Eq. (B1) in a Taylor series, neglecting quadratic terms in $\Delta\xi_1$, and $\Delta\xi_2$. We thus get a homogeneous system of linear equations in $\Delta\xi_1$ and $\Delta\xi_2$ which has nontrivial solutions only if λ satisfies

$$\lambda^2+b\lambda+c=0, \tag{B3}$$

where

$$b=\frac{\Omega_{ei}^2+\Omega_{if}^2}{\Omega_{ei}^2 t_{\mathrm{cav}_1}+\Omega_{if}^2 t_{\mathrm{cav}_2}}(2-f')\ ,$$
$$c=\frac{1}{t_{\mathrm{cav}_1} t_{\mathrm{cav}_2}}(1-f')\ , \tag{B4}$$

and f' is the slope of the gain function [restricted by condition (B2)] at the steady-state value.

If both roots of Eq. (B3) are negative, or have negative real parts, the steady-state values are stable. From Eqs. (B4), one trivially concludes that the stability can be discussed by the simple analysis of the gain-dissipation graphic restricted to condition (B2), as shown in Fig. 4. When the roots of (B3) are complex, we have an oscillatory approach to steady state. From Eqs. (B3) and (B4), this happens when

$$b^2-4c=\left[\frac{\Omega_{ei}^2+\Omega_{if}^2}{\Omega_{ei}^2 t_{\mathrm{cav}_1}+\Omega_{if}^2 t_{\mathrm{cav}_2}}\right]^2 \times[f'^2+(K-4)f'-(K-4)]<0\ , \tag{B5}$$

where

$$K=\frac{4(\Omega_{ei}^2 t_{\mathrm{cav}_1}+\Omega_{if}^2 t_{\mathrm{cav}_2})^2}{(\Omega_{ei}^2+\Omega_{if}^2)^2 t_{\mathrm{cav}_1} t_{\mathrm{cav}_2}}\ . \tag{B6}$$

The inequality (B5) can be satisfied for some value of f' only if

$$K>4\ ,$$

which, from Eq. (B6), is equivalent to the pair of conditions

$$t_{\mathrm{cav}_1}\neq t_{\mathrm{cav}_2}$$

and

$$\left[\frac{\Omega_{t_>}}{\Omega_{t_<}}\right]^4>\frac{t_<}{t_>}\ ,$$

where $t_>$ ($t_<$) is the largest (smallest) damping time and $\Omega_{t_>}$ ($\Omega_{t_<}$) the corresponding coupling time ($\Omega_{t_{\mathrm{cav}_1}}=\Omega_{ei}$, $\Omega_{t_{\mathrm{cav}_2}}=\Omega_{if}$).

APPENDIX C: STABILITY OF THE SEMICLASSICAL SOLUTIONS WITH $\bar{N}_2=0$ AND ZERO DETUNING

Here we discuss the stability of the "one-mode" steady-state solutions

$$\bar{N}_1=\frac{t_{\mathrm{cav}}}{t_{\mathrm{at}}}\sin^2(g\sqrt{\bar{N}_1}\,t_{\mathrm{int}})\ ,$$
$$\bar{N}_2=0 \tag{C1}$$

of Eqs. (3.12) and (3.13). As in the large-detuning case, we change to the variables

$$n_i=\frac{N_i}{t_{\mathrm{cav}}/t_{\mathrm{at}}},\quad i=1,2\ .$$

Then Eqs. (3.12) and (3.13) may be written as follows:

$$\frac{dn_1}{dt}=\frac{n_1}{n_1+n_2}\sin^2\theta\sqrt{n_1+n_2}+\frac{4n_1n_2}{(n_1+n_2)^2}\sin^4\frac{\theta}{2}\sqrt{n_1+n_2}-n_1\ , \tag{C2}$$

$$\frac{dn_2}{dt}=\frac{4n_1n_2}{(n_1+n_2)^2}\sin^4\frac{\theta\sqrt{n_1+n_2}}{2}-n_2\ , \tag{C3}$$

where θ is the "pump parameter," defined in Eq. (3.15). From Eq. (C1) we get for the one-mode steady-state intensity $\bar{n}_1^0$

$$\bar{n}_1^0=\sin^2\theta(\bar{n}_1^0)^{1/2}\ . \tag{C4}$$

From now on, we follow the procedure of Appendix B, linearizing Eqs. (C2) and (C3) around the point $(\bar{n}_1^0,0)$, given by Eq. (C4). We define the parameter λ through

$$n_1=\bar{n}_1^0+e^{\lambda t}\Delta n_1,\quad n_2=e^{\lambda t}\Delta n_2\ . \tag{C5}$$

Expanding Eqs. (C2) and (C3) up to first order in Δn_1 and Δn_2, we get a system of linear equations that has nontrivial solutions for the following values of λ:

$$\lambda_1=\frac{\theta}{2(\bar{n}_1^0)^{1/2}}\sin 2\theta(\bar{n}_1^0)^{1/2}-1\ , \tag{C6}$$

$$\lambda_2=tg^2\frac{\theta}{2}(\bar{n}_1^0)^{1/2}-1\ . \tag{C7}$$

Since we are only considering solutions of Eq. (C4) which correspond to stable one-photon micromaser stationary states, the λ_1 eigenvalue is always negative:

$$\lambda_1<0\ . \tag{C8}$$

If λ_2 is also negative, the one-mode solution is stable, otherwise it is unstable. Thus, from (C7), we arrive at the desired result: the one-mode solution is stable if and only if the Rabi angle is in the first or fourth quadrants:

$$-\pi/2\leq\theta(\bar{n}_1^0)^{1/2}+2k\pi\leq\pi/2;\quad k\in Z\ . \tag{C9}$$

APPENDIX D: SEMICLASSICAL THRESHOLD OF OSCILLATION FOR THE LOWER MODE, WITH ZERO DETUNING

Here we obtain the threshold of oscillation for the lower mode, when $\Delta=0$. In Appendix C we saw that the one-mode solution ($\bar{N}_2=0$) becomes unstable when

$$\theta>\pi/2\ , \tag{D1}$$

although it gets stable again for larger values of θ. Therefore, the critical value of θ fixing the threshold θ_c is at best equal to $\pi/2$. Now we prove that there is no steady-state solution of Eqs. (3.12) and (3.13) with $\bar{N}_2\neq 0$ when

$$\theta\leq\pi/2\ ,$$

so that the critical value is

$$\theta_c=\pi/2 .$$

First, we demonstrate two useful inequalities. Since each atom can emit at best one photon in the average, we get

$$\frac{\bar{N}_i}{t_{\rm cav}}\leq\frac{1}{t_{\rm at}},\quad i=1,2$$

and then

$$\bar{n}_i\equiv\frac{\bar{N}_i}{t_{\rm cav}/t_{\rm at}}\leq 1,\quad i=1,2 . \tag{D2}$$

From Eqs. (3.12) and (3.13) we get the equations for the steady-state intensities $\bar{n}_1$ and $\bar{n}_2$:

$$\bar{n}_1-\bar{n}_2=\frac{\bar{n}_1}{\bar{n}_1+\bar{n}_2}\sin^2\theta\sqrt{\bar{n}_1+\bar{n}_2} , \tag{D3}$$

$$\bar{n}_2=\frac{4\bar{n}_1\bar{n}_2}{(\bar{n}_1+\bar{n}_2)^2}\sin^4\frac{\theta}{2}\sqrt{\bar{n}_1+\bar{n}_2} . \tag{D4}$$

If $\bar{n}_2\neq 0$, we get from Eq. (D4)

$$\frac{\bar{n}_1+\bar{n}_2}{\bar{n}_1}=\frac{4\sin^4\frac{\theta}{2}\sqrt{\bar{n}_1+\bar{n}_2}}{\bar{n}_1+\bar{n}_2} , \tag{D5}$$

and from Eqs. (D3) and (D5)

$$tg^2\frac{\theta\sqrt{\bar{n}_1+\bar{n}_2}}{2}=\frac{\bar{n}_1+\bar{n}_2}{\bar{n}_1-\bar{n}_2}>1 .$$

Therefore, we find that the Rabi angle

$$\theta_R=\theta\sqrt{\bar{n}_1+\bar{n}_2}=g\sqrt{\bar{N}_1+\bar{N}_2}t_{\rm int}$$

must lie in the second or third quadrants:

$$\frac{\pi}{2}<\theta_R+2k\pi<\frac{3\pi}{2},\quad k\in Z \tag{D6}$$

when $\bar{N}_2\neq 0$ (compare with the result in Appendix C about the stability of $\bar{N}_2=0$). Rewriting again Eq. (D4), we get, if $\bar{n}_2\neq 0$,

$$(\bar{n}_1+\bar{n}_2)^2=4\bar{n}_1\sin^4\frac{\theta}{2}\sqrt{\bar{n}_1+\bar{n}_2} . \tag{D7}$$

We look for a solution of Eq. (D7) with $\theta\leq\pi/2$ compatible with the above inequalities. In particular, we want

$$\bar{n}_1\leq 1 , \tag{D8}$$

$$\theta\sqrt{n_1+n_2}>\pi/2 . \tag{D9}$$

Equation (D9) implies that

$$\sqrt{n_1+n_2}>1 . \tag{D10}$$

In Fig. 12 we plot the functions

$$f(\sqrt{n_1+n_2})=(\sqrt{n_1+n_2})^4$$

and

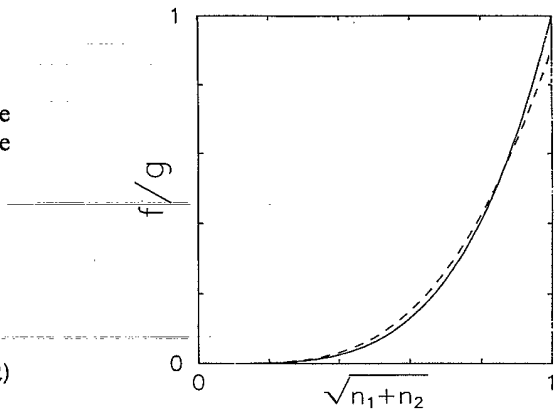

FIG. 12. Semiclassical model of the micromaser with zero detuning: threshold of oscillation of the lower mode. We plot the functions $f(\sqrt{n_1+n_1})=(n_1+n_2)^2$ (solid line) and $g(\sqrt{n_1+n_2})=4n_1\sin^4(\theta/2\sqrt{n_1+n_2})$ (dashed line), where n_1 and n_2 are the normalized mean intensities of the upper and lower modes, respectively, and θ is the pump parameter, defined by Eq. (3.15). $\theta=1.52$ and $n_1=1$. Note that there is no intersection for $\sqrt{n_1+n_2}>1$, fixing the threshold at $\theta=\pi/2$ (see text).

$$g(\sqrt{n_1+n_2})=4n_1\sin^4\left[\frac{\theta}{2}\sqrt{n_1+n_2}\right] ,$$

with $\theta\leq\pi/2$. The roots of Eq. (D7) correspond to the intersections of the curves shown in Fig. 12. We see that if $n_1\leq 1$ [Eq. (D8)], the unique interaction occurs at a value of $\sqrt{n_1+n_2}$ less than unity, violating Eq. (D10), because

$$g(1)=4n_1\sin^4\left[\frac{\theta}{2}\right]\leq 1=f(1)$$

and due to the much stronger increasing of the function f. Therefore, there is no solution of Eq. (D7) which simultaneously satisfies the inequalities (D8) and (D9) when $\theta\leq\pi/2$, thus demonstrating our result.

APPENDIX E: PROOF OF THE STABILITY OF THE SEMICLASSICAL STATE WITH $\bar{N}_1=\bar{N}_2$, ZERO DETUNING

Here we show that the steady state with intensities given by

$$\bar{N}_1=\bar{N}_2=t_{\rm cav}/t_{\rm at} , \tag{E1}$$

at $\theta=n\pi/\sqrt{2}$, n odd, is stable. Following the same procedure of Appendixes B and C, we use the usual renormalized variables

$$\bar{n}_i\equiv\frac{\bar{N}_i}{t_{\rm cav}/t_{\rm at}},\quad i=1,2 \tag{E2}$$

and linearize the zero-detuning equations (C2) and (C3) around the point

$$\bar{n}_1^0=\bar{n}_2^0=1 . \tag{E3}$$

We define the small deviations Δn_1 and Δn_2 through the equations

$$n_1 = 1 + e^{\lambda t}\Delta n_1, \quad n_2 = 1 + e^{\lambda t}\Delta n_2 \ . \tag{E4}$$

Since the gain is stationary under small deviations from the steady state given by Eq. (E3), we get very simple equations for Δn_1 and Δn_2—where the unique contribution comes from the cavity dissipation—when we expand Eqs. (C2) and (C3) around the point given by Eq. (E3):

$$\lambda \Delta n_1 = -\Delta n_1, \quad \lambda \Delta n_2 = -\Delta n_2 \ ,$$

and thus $\lambda = -1$, implying the stability of the steady state.

[1]D. Meschede, H. Walther, and G. Mueller, Phys. Rev. Lett. **54**, 551 (1985).

[2]M. Brune, J. M. Raimond, P. Goy, L. Davidovich, and S. Haroche, Phys. Rev. Lett. **59**, 1899 (1987).

[3]P. Filipowicz, J. Javanainen, and P. Meystre, Phys. Rev. A **34**, 3077 (1986).

[4]M. Brune, J. M. Raimond, and S. Haroche, Phys. Rev. A **35**, 154 (1987).

[5]L. Davidovich, J. M. Raimond, M. Brune, and S. Haroche, Phys. Rev. A **36**, 3771 (1987).

[6]J. H. Eberly, N. B. Narozhny, and J. J. Sanchez-Mondragon, Phys. Rev. Lett. **44**, 1323 (1980); G. Rempe, H. Walther, and N. Klein, Phys. Rev. Lett. **58**, 353 (1987).

[7]P. Filipowicz, J. Javanainen, and P. Meystre, J. Opt. Soc. Am. B **3**, 906 (1986).

[8]P. Meystre, G. Rempe, and H. Walther, Opt. Lett. B **14**, 1078 (1988).

[9]C. R. Carvalho, L. Davidovich, and N. Zagury, Opt. Commun. **72**, 306 (1989).

[10]M. Brune, J. M. Raimond, P. Goy, L. Davidovich, and S. Haroche, IEEE J. Quantum Electron. **QE-24**, 1323 (1988).

[11]H. Heidmann, R. J. Horowicz, S. Reynaud, E. Giacobino, and C. Fabre, Phys. Rev. Lett. **59**, 2555 (1987).

[12]S. Reynaud, C. Fabre, and E. Giacobino, J. Opt. Soc. Am. B **4**, 1520 (1987).

[13]Shi-Yao-Zhu and Xiao-Shen Li, Phys. Rev. A **36**, 3889 (1987).

[14]A. W. Boone and S. Swain, Quantum Opt. **1**, 27 (1989).

[15]L. Sczaniecki, Opt. Acta **27**, 125 (1980); **29**, 69 (1982).

[16]J. Bergou, L. Davidovich, M. Orszag, C. Benkert, M. Hillery, and M. O. Scully, Opt. Commun. **72**, 82 (1989), Phys. Rev. A **40**, 5073 (1989).

[17]M. Sargent III, M. O. Scully, and W. E. Lamb, *Laser Physics* (Addison-Wesley, Reading, MA, 1974).

[18]A. Heidmann, S. Reynaud, and C. Cohen-Tannoudji, Opt. Commun. **52**, 235 (1984).

[19]M. S. Zubairy, Phys. Lett. **87A**, 162 (1982).